Steel and Composite Structures, Vol. 9, No. 2 (2009) 103-118
DOI: http://dx.doi.org/10.12989/scs.2009.9.2.103

Experimental study on repair of corroded steel beam using CFRP

Meiling Chen and Sreekanta Das*

Department of Civil and Environmental Engineering, University of Windsor, Windsor, Ontario N9B 3P4, Canada

(Received October 6, 2008, Accepted October 29, 2008)

Abstract. It has been reported that more than thirty five percent of steel bridges in the USA are structurally deficient because of structural degradations. The degraded structures need either full replacement or rehabilitation such that they are able to provide the required services for a longer period of time. The cost for repair in most cases is far less than the cost of replacement. Moreover, repair method generally takes less time than replacement and also reduces service interruption time. Modern advanced composites have been used in aerospace and automotive fields since World War II. In the recent past, because of the high strength-to-weight ratio and high stiffness-to-weight ratio, these composite materials have been introduced to civil engineering infrastructures primarily for repair and rehabilitation of concrete structures. However, only a few preliminary studies on repair of corroded steel structures using theses composite materials are reported in the literature available in the public domain. Thus, in this study, a series of laboratory tests was undertaken to evaluate the effectiveness of this repair method using carbon fiber reinforced polymer composite. The paper discusses the test method and test results obtained from these tests.

Keywords: steel beam; corrosion; repair; carbon fiber reinforced polymer composite; strength; stiffness; bond; ductility.

1. Introduction

The Federal Highway Administration of the United States of America has developed a program to rate existing bridges on the nation's highways through biannual inspection. At the end of 2007, 35.2% of the steel bridges were classified as structurally deficient (US DOT 2007). The primary reasons for deterioration of the bridges are corrosion, fatigue, and increase in service loads. Similar bridge inventory in Canada could not be found. However, the Province of British Columbia alone owns over 700 structures that are classified as steel bridges and a large of number of them are found to be structurally deficient due to corrosion and aging (Tam and Stiemer 1996). Large temperature fluctuations and extensive use of deicing salts cause serious corrosion in many of these steel and steel-concrete composite bridges.

Various conventional methods for repair of damaged steel members are available. Repair of corroded steel members using steel plate or strip is the most common one. This repair method involves welding or bolting of steel plates or strips onto the existing corroded steel element after cleaning out the corrosive products. Although this method is effective, due to lack of quality control of welds, rivets, and

* Corresponding Author, Email: sdas@uwindsor.ca

bores and due to the introduction of large initial discontinuities, fatigue becomes the major problem for these repaired structures. Moreover, this method often results in stress concentration and thermal locked-in residual stresses which further weaken the repaired and rehabilitated structure (Matta *et al*. 2005).

Recently, Carbon Fiber Reinforced Polymer (CFRP) and other advanced fiber polymers have been introduced in corrosion and other repairs and rehabilitations of structural components. Repair of corroded steel members using CFRP composite involves bonding of the CFRP composite to steel surface using epoxy after proper cleaning. Since no welding or bolting is required when using CFRP composite, this repair method does not affect structure's fatigue life. Cost of CFRP material is higher than the cost of steel plates and strips. However, due to the lightweight of CFRP material and its easy application, this repair method creates savings on labor, and machine and application time. Thus, the repair method using CFRP composite as a whole is still economically comparable to the conventional repair method using steel plate or strip. Since the weight of CFRP is much lighter, repair using CFRP materials does not increase dead weight as much as steel plate does.

Various studies were undertaken on use of CFRP composite for repair and rehabilitation of different concrete structures and these studies were undertaken to achieve increased shear strength, increased flexural strength, and to understand bond behavior between concrete structure and CFRP composite (for example, Meier 1995, Mouring *et al*. 2001, Teng *et al*. 2001, Algusundaramoorthy *et al*. 2003, Harajli and Soudki 2003, Khaled and Sherwood 2003, Lamanna *et al*. 2004, and Kim 2006). Several studies have also been undertaken mostly during last few years for understanding the behavior of strengthened and repaired steel members using various advanced fiber reinforced composites (Gillespie *et al*. 1996, Liu *et al*. 2001, Miller *et al*. 2002, Sayed-Ahmed 2004, Accord and Earls 2006, and Shaat and Fam 2007). Many of these studies focused on the behavior of undamaged and un-corroded steel members strengthened by CFRP composites (Sayed-Ahmed 2004, Accord and Earls 2006, and Shaat and Fam 2007). However, only very limited and preliminary test data on repair of corroded steel member using CFRP composite are available in the open literature (Gillespie *et al*. 1996, Liu *et al*. 2001, and Miller *et al*. 2002). Majority of all these studies focused primarily on the strength and elastic stiffness of repaired and rehabilitated steel members and very little or no attention was paid to study the ductility of repaired beams and bond between steel and CFRP composites.

Accord and Earls (2006) in their numerical study found that the application of glass fiber reinforced polymer (GFRP) composite on the compression flange of cantilever I-shaped steel beams increases both strength and ductility. This increase occurs mainly because the failure mode of the retrofitted steel beams changes from local buckling to lateral torsion buckling. They also found that strategic placement and sizing of GFRP sheets can provide even higher ductility and strength. Their study focused on application of GFRP on compression flange of undamaged (un-corroded) beams. The current study, however, was undertaken primarily to determine the feasibility and effectiveness of repair method for corrode (damaged) steel beam that has developed corrosion on its tension flange using CFRP composite. Special attention was paid to study the requirement of optimum width and thickness of CFRP composite required for restoring the strength and elastic stiffness to the level of virgin beam with maximum possible ductility and without causing any major bond failure. This study was undertaken based on laboratory tests on corroded steel I-shaped beams.

2. Brief overview of the contents of the manuscript

An experimental study was undertaken to study the feasibility and effectiveness of the repair method

for corroded flexural steel beams using the carbon fiber reinforced polymer (CFRP) composite. This paper discusses the results obtained from corroded steel beams repaired with CFRP fabrics. The following key issues were studied and presented in this paper.

1. Develop a suitable and easy-to-apply arrangement for CFRP placement such that the global debonding between CFRP composite and steel substrate is completely eliminated to avoid the premature failure and collapse of corroded flexural steel beam repaired with CFRP composite.
2. Design a suitable method for making up (filling the gap) the thickness loss of steel beam and at the same time ensuring no debonding at and near the corrosion zone.
3. Determine best layout and geometry (width and length) of CFRP composite to achieve the strength and elastic stiffness to the level of virgin (undamaged) flexural beam and to obtain good ductility at the same time.

3. Experimental procedure and materials

A test program with nine full-scale tests was designed and undertaken to study the effectiveness of repair technique using carbon fiber reinforced polymer (CFRP) fabrics as shown in Table 1. The specimens are identified by their specific names. The CV, CC, and RC in their names denote Control Virgin (un-corroded) specimen, Control Corroded (damaged) specimen, and Repaired Corroded specimen, respectively. For repaired specimens, longer names were required. For example, for specimen RC-W80-T2.4-G1, W80 and T2.4 indicate that 80 mm wide and 2.4 mm thick CFRP composite was used. The last letter, G1, indicates that the specimen belongs to group one.

The schematic of test setup is shown in Fig. 1. A pin-roller boundary condition was used for all the specimens. The specimens were separated in two groups. The specimens in group 1 did not have any additional strips to stiffen the web and top flange. However, additional steel strips to stiffen the top flange and the web (Fig. 1) under the load application point were welded on all the specimens of group 2 to reduce premature web and flange buckling at mid-span. A steel strip of 1000 mm long × 110 mm wide × 3 mm thick was welded to the top flange of each specimen of group 2 to minimize the top flange buckling. A 170 mm long steel strip was welded on either side of the web at the mid-span of all specimens of group 2 to minimize buckling in the web at mid-span. The specimens of both groups were however, supported laterally at four brace points along the length (direction 3), as shown in Fig. 1, to minimize lateral torsional buckling failure.

Table 1 Test matrix for specimens

Specimen number	Specimen name	Group	CFRP width (mm)	CFRP thickness (mm)	Web strips	Flange strip
1	CV-G1	1	0	0	No	No
2	CC-G1		0	0	No	No
3	RC-W80-T2.4-G1		80	2.4	No	No
4	RC-W133-T2.4-G1		133	2.4	No	No
5	CV-G2	2	0	0	Yes	Yes
6	CC-G2		0	0	Yes	Yes
7	RC-W133-T2.4-G2		133	2.4	Yes	Yes
8	RC-W133-T1.2-G2		133	1.2	Yes	Yes
9	RC-W133-T0.6-G2		133	0.6	Yes	Yes

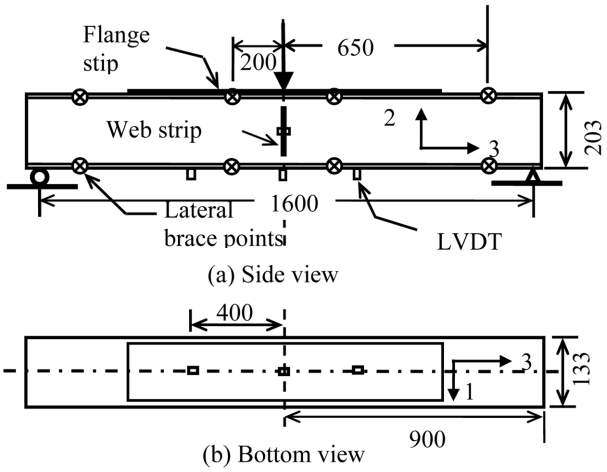

Fig. 1 Test setup and locations of LVDTs

Standard wide flange W200 × 21 beam (equivalent imperial designation is W8x14) as specified in Canadian Standard (CSA 2004) was used in this study. The total depth and width of flange of this beam section are 203 mm and 133 mm, respectively. The web and flange thicknesses are 5 mm and 6.4 mm, respectively. Total length and span of the specimens were 1800 mm and 1600 mm, respectively (Fig. 1). Specimen length was chosen such that the beam does not experience lateral torsional buckling. However, the first test on a virgin (undamaged) specimen showed that the beam experienced lateral torsional buckling when the section reached its moment of resistance. At that time, vertical deformation at mid-span was only 9.3 mm. The test data of this beam specimen is not reported in this paper. Because of early lateral torsional buckling in this specimen, stiffeners at four brace points as shown in Fig. 1 in all subsequent nine specimens (Table 1) were used to minimize the lateral torsional buckling. As a result, the beam specimen showed an increased load carrying capacity and ductility and these are discussed later in this paper.

Three-point bending load was applied on each of these specimens. Concentrated load was applied on the top flange of the specimen at its mid-span using a load control method until the specimen yielded. Then, load was applied using a stroke control method and loading was continued until either the specimen failed or when the vertical deformation at mid-span reached in the range of 30 mm to 35 mm to avoid damages in the equipment and test setup. A failure in this study was identified at the first occurrence of severe lateral torsional buckling or severe buckling of web or severe flange buckling or rupture of steel or rupture of CFRP matrix or severe debonding of CFRP composite that caused sudden drop in load carrying capacity of the specimen.

3.1. Shape of corrosion

A circular arc-shaped surface corrosion at the mid-span of bottom flange was simulated by machining. Length of corrosion was 100 mm long in direction-3 and it was symmetric about the mid-span of the specimen. The plan view of the corrosion was trapezoidal. Fig. 2 is the three-dimensional sketch of the corrosion. The length of the corrosion was 100 mm long at the edge of the flange and 80 mm long at the web-flange connection in the longitudinal direction of the beam (direction-3). The width of the corrosion was 64 mm along the width of the beam (direction-1) as shown in Fig. 2. The corrosion

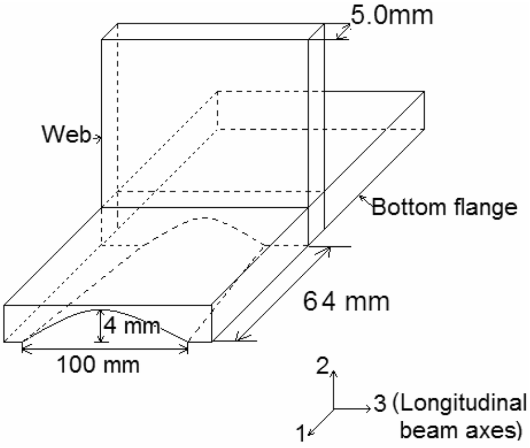

Fig. 2 A 3-D sketch of corrosion

was simulated over the half of the flange width. Thus, the corrosion was symmetrical about the mid-span of beam in direction-3, but was unsymmetrical in direction-1. Variation of corrosion depth in direction-3 was between 4 mm at its mid-length to no corrosion at its ends (Fig. 2) and variation in corrosion depth in direction-1 was from 4 mm at the edge of flange to 2.6 mm at the web-flange intersection. The reduction of 4.7% in bending stiffness of the beam's cross-section at its mid-span occurred due to the corrosion.

3.2. Group 1 specimens

Four lateral supports were installed on each side of every specimen in both groups as discussed earlier. Specimens 1 through 4 belong to group 1. The first specimen in this group (specimen 1 in Table 1) was a control and virgin (no corrosion) specimen and the second specimen (specimen 2 in Table 1) was a control but corroded (damaged) specimen. The remaining two specimens (specimens 3 and 4 in Table 1) were corroded specimen similar to specimen 2 but repaired with 2.4 mm thick CFRP composite. Specimen 3 (RC-W80-T2.4-G1) was repaired with 80 mm wide CFRP composite which covered 60% of the flange width. However, specimen 4 (RC-W133-T2.4-G1) was repaired with 133 mm wide CFRP composite and thus, whole flange width was covered with the CFRP composite even though the corrosion was over half of the flange width only. The width of corrosion was 64 mm. The objective of this was to study the influence of width of CFRP composite on load carrying capacity, ductility, and elastic stiffness of the repaired specimens, and influence on the effectiveness of bond between steel and CFRP composite. The repaired specimens in group1 failed either due to buckling of web or flange at mid-span where load was applied or due to CFRP debonding. Top flange under the load also buckled towards the end of the tests. Therefore, additional steel strips were welded to stiffen the web and the top flange of all the specimens of group 2.

3.3. Group 2 specimens

Last five specimens (specimens 5 through 9) in Table 1 belong to this group. The first specimen (specimen 5 or CV-G2) was the control and virgin (no corrosion) specimen and the second specimen

(specimen 6 or CC-G2) was the control but corroded (damaged) specimen of group 2. These specimens are identical to the specimen 1 (CV-G1) and specimen 2 (CC-G1), respectively except the top flange and web at the mid-span of specimens in group 2 were stiffened. The last three specimens in the table (specimens 7 through 9) were corroded specimens but repaired with CRFP composite. The only difference among these three specimens was the total thickness of CFRP composite applied to them. Specimens 7, 8, and 9 were repaired with 2.4 mm, 1.2 mm, and 0.6 mm thick CFRP composite, respectively. The objective of this was to study the influence of thickness of CFRP composite on the load carrying capacity, ductility, and stiffness of the rehabilitated specimens, and influence on the bond behavior. Since the top flange and web under the load was stiffened, these specimens did not fail either due to flange buckling or due to buckling of web at the mid-span.

The average length of CFRP composite (direction-3) was 1,000 mm and it was kept unchanged for all specimens of both groups. Each layer was 6 mm shorter than the next layer to avoid peeling and debonding actions at the CFRP termination points. Further, five 50 mm wide and 0.3 mm thick cross-wraps (direction-1) made from same CFRP composite at spacing of 220 mm centers (Fig. 3) were applied to all repaired specimens of both groups to avoid premature debonding of longitudinal CFRP composites. The cross-wraps were extended almost up to the mid-depth of the beam. The radius of cross-wraps at the flange-web intersection was same as the radius of the fillet. Short pieces (100~115 mm long and 25~50 mm wide) of CFRP composite were used to fill the corrosion depth and to eliminate discontinuity between CFRP composite and steel. These short CRRP composite pieces were not meant for enhancing either the load carrying capacity or stiffness of the repaired beam specimens.

3.4. Material properties

Structural steel beam was used in this study. The yield strength, ultimate strength, and modulus of elasticity of the beam's steel were obtained as 420 MPa, 550 MPa, and 215 GPa, respectively. The strain at rupture was recorded as 33%. The average tensile modulus and average rupture strain of the CFRP dry fabric were obtained as 227 GPa and 4.3%, respectively. Only unidirectional CFRP fabric was used.

3.5. Preparation and application of CFRP

First, the steel surface was sandblasted to "white metal" finish by sand blasting using 12~20 mesh industrial coarse sand. The surface was then cleaned using compressed air to ensure good bonding between CFRP composite and steel substrate. Then, a thin layer of primer was applied on the steel substrate to enhance the bond. However, no special chemical treatment was applied to enhance the bonding. Next, the CFRP composite of required dimensions (length and width) was impregnated in the resin before it

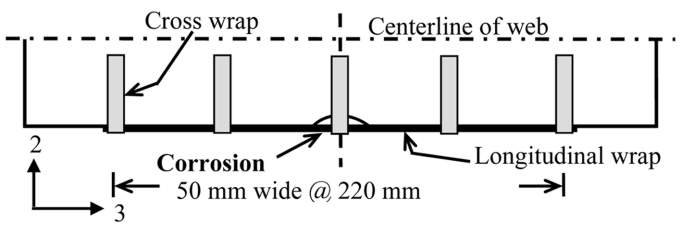

Fig. 3 Longitudinal and cross CFRP composites

was placed on the steel substrate. The required thickness of CFRP was achieved using multi layers of CFRP dry fabrics. The average length of CFRP composite was kept same (1000 mm) for all rehabilitated specimens. However, the thickness and width of CFRP composites were changed (Table 1). The beams repaired using CFRP composites were air cured for a week before undertaking the load test.

3.6. Instrumentation

Electrical resistance strain gauges, LVDT (linear variable differential transformer), load cell, hydraulic pump, loading jack, and computer data acquisition system were used for applying load and acquiring strain, load, and displacement data. The LVDTs were used to acquire deformation data. A total of four LVDTs were used for each beam specimen. Three of them were installed at the bottom flange to obtain the vertical deformation of the beam and the fourth one was installed at the mid web height of mid-span of the beam (Fig. 1) to obtain the lateral deformation.

Strain gauges of two different gauge lengths, 3 mm and 13 mm, were used for measuring strains on steel substrate and strains on CFRP composites, respectively. Strain gauges were used to study the effectiveness of bond between the steel substrate to the CFRP composites and thus, no strain data were acquired from control virgin and control corroded specimens. A total of five 3 mm long strain gauges were installed on the top surface of the bottom flange as shown by S1 through S5 in Fig. 4. Another five strain gauges of 13 mm gauge length were installed on the CFRP composite and they are shown by C1 through C5 in Fig. 4. Effort was made to position each strain gauge pairs, such as C5 and S5, on the same vertical axis (direction-2) as shown in this figure.

A loading jack of 450 kN capacity with a load cell of same capacity was used along with an hydraulic pump to apply load and acquire the load data from the tests. All the test data were acquired through a computer data acquisition system. Two load cells of 225 kN capacity each were also installed on the supports to monitor and ensure equal load distributions between the two supports.

4. Results and discussions

4.1. Load-deformation behaviors of group 1

Fig. 5 shows the load-deformation behavior for specimens in gruop1. The numbers beside the curves

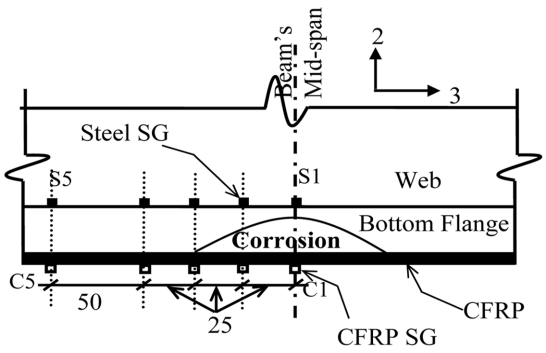

Fig. 4 Locations of strain gauges

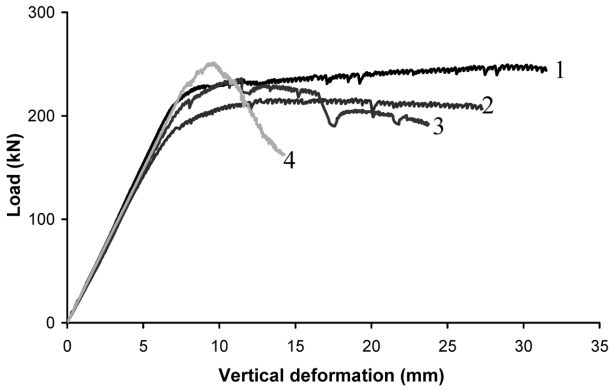

Fig. 5 Load-deformation of group 1 specimens

indicate the specimen numbers as shown in Table 1 and thus, 1 is for the first specimen (CV-G1) and 4 is for the fourth specimen, RC-W133-T2.4-G1. The first specimen (CV-G1) yielded at 202 kN load and 7 mm vertical deformation at mid-span. The ultimate load was recorded as 249 kN when the vertical deformation was 29 mm. This beam specimen exhibited good ductility since it was able to show large elastic-plastic deformation. The test was discontinued at 243 kN and the vertical deformation at 31.5 mm (Table 3). This specimen did not fail either due to lateral torsion buckling or due to web buckling. However, the top flange under the load buckled slightly at this stage. The specimen at that time was considered as failed and the test was discontinued primarily due to large deformation.

The second specimen (CC-G1) in Table 1, the other control specimen with corrosion and shown by 2 in Fig. 5, was also able to show good elastic-plastic deformation. This specimen however, yielded at a lower load of 165 kN load and at that time vertical deformation at mid-span of the beam was recorded as 5.7 mm. The drop in yield load with respect to the virgin specimen (specimen 1) was 18.3% as shown in Table 2. The ultimate load was recorded as 215 kN (Table 2) which was 13.6% lower as compare to specimen 1 (CV-G1) and at that time, the mid-span vertical deformation was recorded as 13.4 mm. In this table, P_y is the yield load, P_{ult} is the ultimate or maximum load. The changes in yield and ultimate loads were calculated with respect to the respective values obtained from specimen 1 or virgin specimen (CV-G1). The specimen first yielded at the corrosion location and it was confirmed since significant necking at that location was observed. Then, the flange and a small portion of the web under the load buckled plastically. The specimen was considered as failed and the test was discontinued when the vertical deformation at mid-span of the beam reached 27.3 mm since the buckling at the web-flange intersection at mid-span became large.

Table 2 Load and failure modes group1 specimens

Loads and Failure modes	Specimen number			
	(1)	(2)	(3)	(4)
P_y (kN)	202	165	200	227
P_{ult} (kN)	249	215	238	249
Change in P_y (%)	00.0	−18.3	−01.0	+12.4
Change in P_{ult} (%)	00.0	−13.6	−04.4	+00.0
Failure mode	Flange buckling	Flange-web buckling	CFRP debonding	Severeweb buckling

The third specimen (RC-W80-T2.4-G1) of group 1 was a corroded specimen repaired with 80 mm wide CFRP composite covering 60% of the width of the flange. Thickness of CFRP composite was 2.4 mm. The objective of this test was to study the effectiveness of this repair technique when the CFRP is not applied over the full flange width. This specimen yielded at a load of about 200 kN and when maximum vertical deformation was 6.7 mm. The ultimate load was recorded as 238 kN and at that time the maximum vertical deformation reached 11 mm. Thus, this specimen was not able to restore the ultimate strength to the level of the virgin specimen (CV-G1). After passing the ultimate load capacity and at about 17 mm mid-span vertical deformation, loud debonding noise was heard and the load capacity dropped suddenly to a level lower than the load carrying capacity of control corroded specimen (CC-G1). At that time, it was observed that the CFRP composite debonded at its longitudinal termination line at the mid-span of the beam. However, the specimen continued to deform in a stable manner and load capacity continued to drop gradually until the maximum vertical deformation reached 23.7 mm and load dropped to 192 kN. At this point, the debonding became sever and the longitudinal (direction-3) and transverse (direction-1) CFRP fibers ruptured (Fig. 6). It should be noted that only a thin layer (0.3 mm thick) of unidirectional CFRP composite was used for the cross-wraps. At this stage the specimen was considered failed and the test was discontinued.

The last specimen (specimen 4 or RC-W133-T2.4-G1) in group 1 was repaired same way as it was done for the specimen 3. The only difference between these two specimens was the width of CFRP composite. The width of CFRP composite for specimen 4 was 133 mm whereas the width of CFRP composite for specimen 3 was 80 mm. The ultimate load capacity of specimen 4 was same as it was for the control virgin (CV-G1) specimen (Table 2). However, the ultimate load carrying capacity of specimen occurred at a much smaller mid-span vertical deformation and the deformation at that time was recorded as 9.6 mm. It should be noted that the ultimate load capacity for the control virgin specimen was recorded when the mid-span vertical deformation was 29 mm. Soon after reaching the ultimate load capacity, buckling of the web of specimen 4 at its mid-span initiated causing a rapid drop in its load capacity. The specimen was considered to be failed due to sever web buckling at mid-span when maximum vertical deformation reached 14.2 mm and load capacity dropped to 162 kN (Fig. 5). Thus, the ductility of this specimen reduced by 55% which was a significant drop as compare to the control virgin specimen (CV-G1) and this specimen exhibited least ductility in this group though its ultimate load capacity was same as what was observed from the control virgin specimen. The ductility in this paper refers to the ability to deform elastic-plastically.

A 7.3% drop in elastic stiffness for the control corroded specimen (CC-G1) occurred as compare to

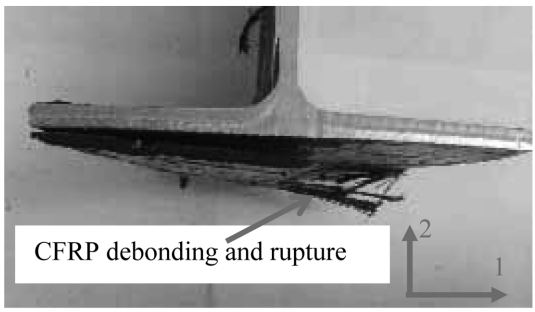

Fig. 6 Rupture of CFRP composite at mid-span

Table 3 Stiffness and ductility of group1 specimens

Stiffness and Ductility	Specimen number			
	(1)	(2)	(3)	(4)
Load-deformation stiffness (kN/m)	30.3	28.1	29.3	30.6
Load-deformation stiffness change (%)	00.0	−7.3	−3.3	1.0
Deformation at failure (mm)	31.5	27.3	23.7	14.2
Change in deformation (%)	00.0	−13.3	−24.8	−55.0

control virgin specimen (Table 3). Both repaired specimens (specimens 3 and 4) however, were able to restore the elastic stiffness to some extent. Specimen 4 was able to restore the elastic load-deformation stiffness to the level of control virgin specimen. The ductility in both repaired specimens reduced and the reductions were 24.8% and 55%, respectively. Specimen 4, which was repaired with 133 mm wide CFRP composite, lost the ductility most.

Thus, specimen 4 was able to restore the ultimate load carrying capacity and elastic load-deformation stiffness to the level of the virgin specimen (CV-G1). However, the ductility dropped significantly. Therefore, this repaired beam may be considered as acceptable only if the ductility requirement of the repaired beam is not important. Specimen 3 was not able to restore the ultimate load carrying capacity to the level of virgin specimen. Further, this specimen exhibited major debonding of CFRP composite when the mid-span deformation was only 17 mm and soon after the repair method became ineffective. Thus, specimen 3 which was repaired covering partial width of the flange is not an acceptable option.

4.2. Strain behaviors of specimens 3 and 4

Figs. 7 and 8 show strain data for strain gauges at location 5 (Fig. 4) for specimen 3 and specimen 4, respectively. Both steel and CFRP gauges experienced a linear increase in strain values until specimen yielded (line A in Figs. 7 and 8). This indicates that perfect bonding between CFRP composite and steel substrate was achieved until the specimen yielded. The slopes of strain-deformation relationship obtained from CFRP gauges were slightly higher than the slopes obtained from respective steel gauges because of strain compatibility. Then, the strains in CFRP gauges continued to increase whereas the strain

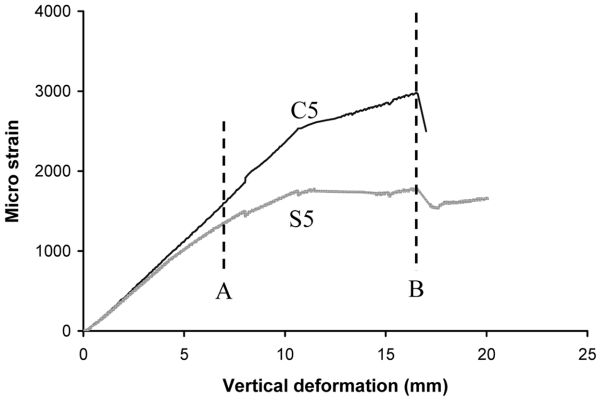

Fig. 7 Deformation-strain for specimen 3

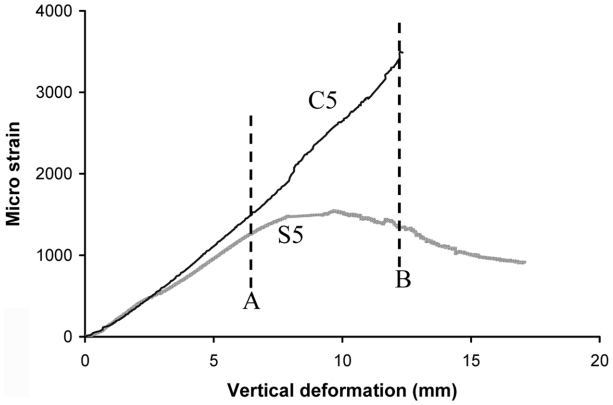

Fig. 8 Deformation-strain for specimen 4

in steel stabilized and then reduced slightly. This indicates that the yielding in steel occurred and strain localized away from the gauge location 5 and thus, the strain steel gauges at location 5 stabilized and reduced (relaxed) once the beam yielded. Good bond between steel surface and CFRP composite maintained even after steel yielded since no sudden change in strains was observed.

However, for specimen 3, at about 17 mm mid-span vertical deformation (line B in Fig. 7), the CFRP composite debonded over a longer area and thus, strain in CFRP gauge dropped suddenly and the strain gauge failed soon after. At this point, load from steel to CFRP was transferred through other areas where the bond between steel and CFRP composite was still good and the load transfer continued until the specimen failed due to rupture in the CFRP fibers. Specimen 4 did not experience any major debonding between CFRP composite and steel and thus, a similar drop in CFPR strain gauge did not occur. The CFRP strain gauge failed when strain reached about 3500 micro strain (line B in Fig. 8) which was the limit of the gauges used in this study.

4.3. Load-deformation behaviors of group 2

Fig. 9 shows load-deformation behavior for specimens of group 2. Specimen 5 (CV-G2) is the first

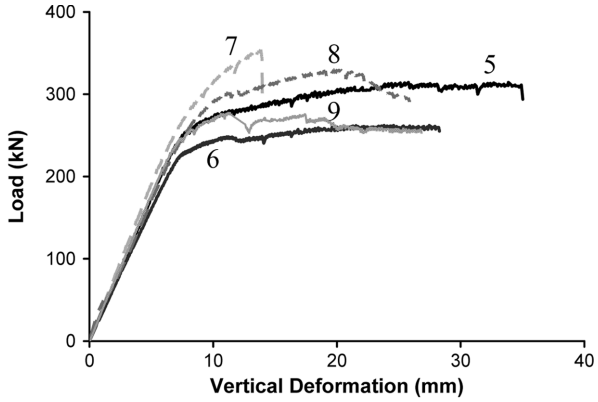

Fig. 9 Load-deformation of group 2 specimens

specimen of group 2 and it was the control virgin (un-corroded) specimen for this group (Table 1). Specimen 6 (CC-G2) was the control corroded specimen. Both specimens were able to show good ductile behavior. The ultimate load carrying capacities for these two specimens were obtained as 314 kN and 260 kN, respectively. Thus, ultimate load carrying capacity of the corroded control specimen (specimen 6) dropped by 17.2% (Table 4) and the ductility dropped by 20% (Table 5). Specimen 5 (CV-G2) failed due to sever web buckling at the roller support when mid-span vertical deformation reached 35 mm whereas, specimen 6 (CC-G2) failed due to rupture of steel at the corrosion when the vertical deformation was 28 mm (Fig. 8).

Specimen 7 (RC-W133-T2.4-G2) was the first repaired specimen of this group. Total thickness of CFRP composite for this specimen was 2.4 mm which was the thickest among all the specimens. As result of this, for this specimen, the stiffness of elastic part of load-deformation behavior and ultimate load carrying capacity were the largest (Tables 4 and 5). The ultimate load carrying capacity for this specimen was 12.7% higher than that of control virgin specimen (CV-G2) (Table 5). However, the ductility of this specimen was the least and the ductility was 60.6% lower than the control virgin specimen (CV-G2). Thus, this specimen can be considered as acceptable only if the ductility requirement of the beam is not important. No debonding was observed in this specimen.

Specimen 9 (RC-W133-T0.6-G2) was the last specimen in this group. This specimen was repaired same way as it was done for specimen 7. However, thickness of the CFRP composite used in this specimen was the least and it was 0.6 mm. The ultimate load capacity was obtained as 276 kN (Table 4) when the vertical deformation was about 12 mm. Thus, a reduction in load carrying capacity of 12.1% was observed in this specimen. Soon after, the cross-wrap CFRP composite on the corrosion ruptured which created a loud noise and thus, the load capacity dropped. The drop in load capacity continued until it matched the capacity of control corroded specimen (CC-G2). The drop in load carrying capacity occurred due to initiation of rupture of longitudinal CFRP composite. This specimen finally failed when the vertical deformation was 26.8 mm because longitudinal CFRP fibers and steel ruptured at mid-span of the beam. The ductility of this specimen was therefore, 23.4% lower even though the elastic stiffness was slightly higher than the control virgin specimen (CV-G2) (Table 5). Thus, the repair for this specimen

Table 4 Loads and failure modes of group 2 specimens

Loads and Failure modes	Specimen number				
	(5)	(6)	(7)	(8)	(9)
P_y (kN)	233	212	255	250	215
P_{ult} (kN)	314	260	354	330	276
Change in P_y (%)	00.0	-09.0	+9.4	+7.3	-07.7
Change in P_{ult} (%)	00.0	-17.2	+12.7	+05.1	-12.1
Failure mode	Severe web buckle	Steel rupture	Severe web buckle	Severe web buckle	Steel-CFRP rupture

Table 5 Stiffness and ductility of group 2 specimens

Stiffness and Ductility	Specimen number				
	(5)	(6)	(7)	(8)	(9)
Load-deformation stiffness (kN/m)	34.8	32.3	37.6	36.1	35.3
Load-deformation stiffness change (%)	00.0	−07.3	+08.0	+3.7	+1.4
Deformation at failure (mm)	35.0	28.0	13.8	25.9	26.8
Change in deformation (%)	00.0	−20.0	−60.6	−26.0	−23.4

was not effective. However, no debonding between CFRP composite and steel was observed in this specimen.

Specimen 8 (RC-W133-T1.2-G2) showed most promising behavior among all the repaired specimens of both groups. This specimen was repaired with 1.2 mm thick CFRP composite, which increased the elastic load-deformation stiffness by 3.7%. The ultimate load for this specimen was 330 kN which was 5.1% higher than the control virgin specimen (CV-G2). The specimen was considered to be failed when the vertical deformation was 25.9 mm due to sever web buckling at roller support which was far away from the repaired zone. Thus, the ductility for this specimen was 26% lower than the control virgin specimen. It should be noted that no failure occurred at and near the repaired zone when the test was discontinued. A mild debonding noise was heard when the vertical deformation was about 13 mm and the load dropped slightly. However, the load capacity restored soon after that and this indicates that a minor and localized debonding occurred at that stage which seems not to influence the global load-deformation behavior much (Fig. 9). The beam was sectioned at its mid-span and at every 50 mm distances after the test was completed to examine if any major debonding occurred in this specimen. Only one small and very localized debonding was found near the end of the flange at its mid-span (Fig. 10). No other debonding was found. Thus, this specimen exhibited the best performances for strength, ductility, and bond between CFRP composite and steel.

Specimen 6 (CC-G2), the control corroded specimen of group 2, showed a drop of 7.3% in its elastic load-deformation stiffness. However, the specimen 8 (RC-W133-T1.2-G2) showed an increase of 3.7% in its elastic load-deformation stiffness. The specimen 8 was repaired with 1.2 mm thick CFRP composite whereas, the depth of corrosion at mid-span varied from 4 mm to 2.6 mm. Thus, it seems that the filler short CFRP composites contribute to the elastic load-deformation stiffness to some extent even though they were not meant for this.

4.4. Strain behavior of specimen 8

Fig. 11 shows mid-span vertical deformation vs. strain behavior of all CFRP strain gauges and Fig. 12 shows similar behavior for all steel strain gauges used in specimen 8. The strain gauge numbers and their locations are shown in Fig. 4. The strain gauge numbers are also indicated in Figs. 11 and 12. The strains at gauges C1 and S1 showed highest rate of strain since these two gauges were located at the mid-span of beam and thus, at the mid-length of the corrosion. The strains on gauges 5 (C5 and S5)

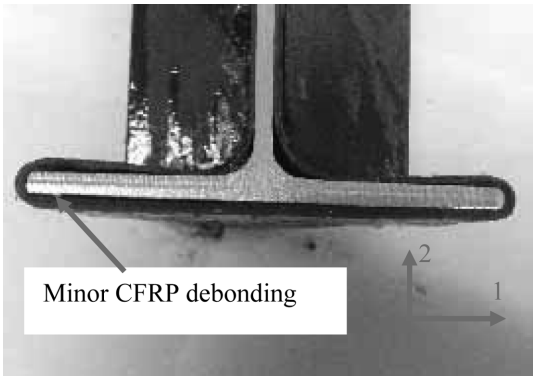

Fig. 10 Section of specimen 8 at mid-span

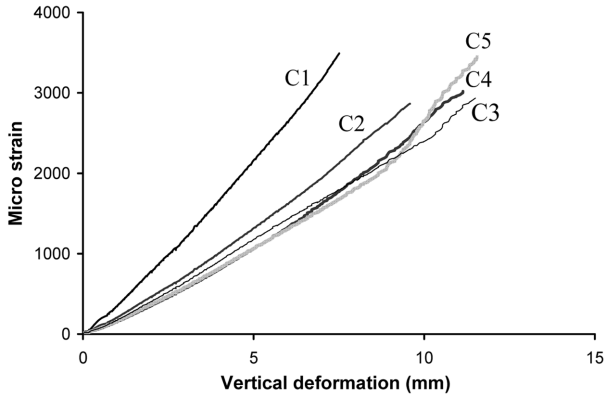

Fig. 11 Deformation-CFRP strain for specimen 8

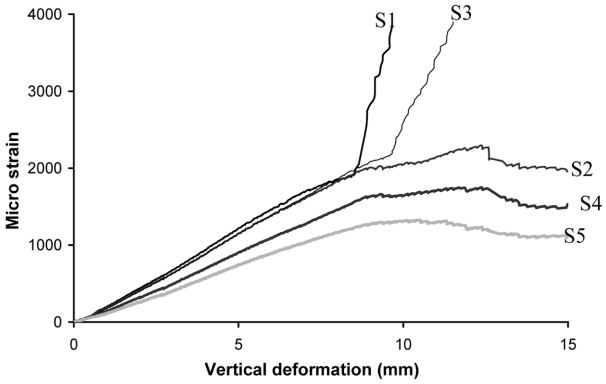

Fig. 12 Deformation-steel strain for specimen 8

showed lowest strain rate until the beam behavior was linear and elastic since these gauges were the most remote ones from the corrosion. The strains in steel gauges S1 and S3 started to increase at faster rates when the vertical deformation reached about 8 mm and this confirms that at this stage, the yielding in steel localized at locations 1 (mid-length of corrosion) and 3 (at the end of corrosion) and thus, strains in other steel gauges (S2, S4, and S5) stabilized and reduced slightly. However, the CFRP gauges maintained almost same strain rates until the gauges failed. Both steel and CFRP strain gauges failed when strain value reached a value between 3000 and 4000 micro strains because of the limits of these gauges. The strain plot in Fig. 11 indicates that the good bonding between the CFRP composite and steel surface was achieved until those gauges failed. This is also apparent from the load-deformation behavior in Fig. 9.

4.5. Vertical deformations of specimen 8

Fig. 13 shows vertical deformation distribution in direction-3 obtained from three LVDTs (Fig. 1) mounted at 400 mm spacing on the bottom flange of specimen 8. Four curves represent deformation

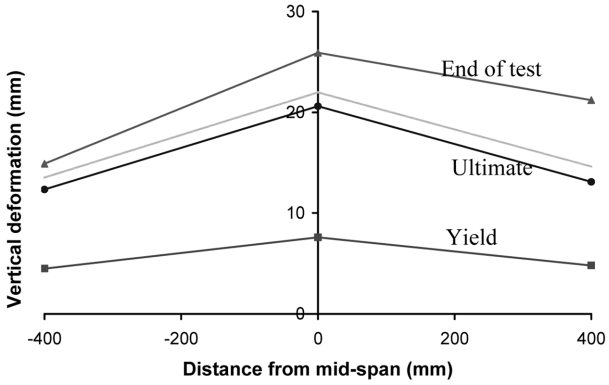

Fig. 13 Distribution of vertical deformation for specimen 8

distributions when yield load (250 kN) was applied, when ultimate load (330 kN) was applied, when mid-span vertical deformation was 22 mm, and when specimen failed and test was discontinued (mid-span vertical deformation was 25.9 mm). This figure shows that the vertical deformations recorded from this specimen were almost symmetric about the beam's mid-span until when the mid-span vertical deformation was 22 mm. At that stage, the buckling in the web on the roller end initiated and thus, the vertical deformation distribution became un-symmetric and this un-symmetry increased as mid-span deformation was increased. Thus, the deformation test data confirms that this beam specimen behaved in a very stable manner until about 22 mm mid-span vertical deformation. The load capacity dropped at a faster rate then after because the web buckling on the roller end initiated and grew with application of further deformation.

5. Conclusions

The following conclusions are made based on the experimental results obtained from this study. The conclusions made are specific to the steel beam, corrosion shape, and loading procedure used in this study.

1. Flexural steel beams which developed corrosion on its tension flange can be repaired effectively and successfully using CFRP composite. However, optimum thickness and optimum width of the composite are to be used and major bond failure needs to be prevented.
2. The CFRP composite needs to be applied over the full flange width even when the corrosion is not spread over the full flange width.
3. The optimum thickness of CFRP composite for the corroded beams used in this study was found to be 1.2 mm though the maximum depth of corrosion was 4 mm.
4. It seems that the short pieces of longitudinal CFRP composite which were used to fill the corrosion gap together with the 50 mm wide transverse CFRP wrap contributed additional stiffness to the repaired specimens. Thus, it seems that filling of corrosion with same CFRP composite is beneficial.
5. Major bond failure was successfully avoided and excellent bond between CFRP composite and steel substrate was obtained in this study by applying 1000 mm longitudinal CFRP composite over full flange width and 50 mm wide cross warps at every 220 mm centers.

Acknowledgement

The authors acknowledge the financial support received from the Natural Sciences and Engineering Research Council of Canada (NSERC).

References

Accord, N.B. and Earls, C.J. (2006), "Use of fibre-reinforced polymer composite elements to enhance structural steel member ductility", *J. Compos. Constr.*, **10**(4), 337-344.

Algusundaramoorthy, P., Harik, I.E. and Choo, C.C. (2003), "Flexural behavior of R/C beams strengthened with carbon fiber reinforced polymer sheets or fabric", *J. Compos. Constr.*, **7**(4), 292-301.

Canadian Standards Association (CSA) (2004), *CSA G40.20-04/G40.21-04: General Requirements for Rolled or Welded Structural Quality Steel/ Structural Quality Steel*, CSA, Mississauga, Ontario, Canada.

Gillespie, J.W. Jr., Mertz, D.R., Kasai, K., Edberg, W.M., Ammar, N., Kasai, K. and Ian, C. (1996), "Rehabilitation of steel bridge girders through application of composite materials", *Proc. of the 28th Int. SAMPE Technical Conf.*, Seattle, USA, 1249-1257.

Harajli, M. H. and Soudki, K.A. (2003), "Shear strengthening of interior slab-column connections using carbon fiber-reinforced polymer sheets", *J. Compos. Constr.*, **7**(2), 145-153.

Khaled, S. and Sherwood, T. (2003), "Bond behavior of corroded steel reinforcement in concrete wrapped with carbon fiber reinforced polymer sheets", *J. Mater. Civil Eng.*, **15**(4), 358-370.

Kim, I.S. (2006), "Rehabilitation of Poorly Detailed RC Structures Using CFRP Materials", Master's Thesis, The University of Texas at Austin, Austin, Texas, USA.

Lamanna, A. J., Bank, L. C. and Scott, D. W. (2004), "Flexural strengthening of reinforced concrete beams by mechanically attaching fiber-reinforced polymer strips", *J. Compos. Constr.*, **8**(3), 203-210.

Liu, X., Silva, P.F. and Nanni, A. (2001), "Rehabilitation of steel bridge members with FRP composite materials", *Proc. Int. Conf. on Composites in Construction*, Porto, Portugal, 613-617.

Matta, F., Karbhari, V. M. and Vitaliani, R. (2005), "Tensile response of steel/CFRP adhesive bonds for the rehabilitation of civil structures", *Struct. Eng. Mech.*, **20**(5), 589-608.

Meier, U. (1995), "Strenthening of structures using carbon fibre/epoxy composites", *Constr. Build. Mater.*, **9**(6), 341-351.

Miller, T.C., Chajes, M. J., Mertz, D. R. and Hastings, J. N. (2002), "Strengthening of a steel bridge girder using CFRP plates", *J. Bridge Eng.*, **6**(6), 514-522.

Mouring, S.E., Barton, O. and Simmons, K.D. (2001), "Reinforced concrete beams retrofitted with advanced composites", *Adv. Compos. Mater.*, **10**(2), 139-146.

Sayed-Ahmed, E.Y. (2004), "Strengthening of thin-walled steel section beams using CFRP strips", *Proc. of the 4th Advanced Composites for Bridges and Structures*, Calgary, Canada.

Shaat, A. and Fam, A. (2007), "Finite element analysis of slender HSS columns strengthened with high modulus composites", *Steel Compos. Struct.*, **7**(1), 19-34.

Tam, C.K. and Stiemer, S.F. (1996), "Development of bridge corrosion cost model for coating maintenance", *J. Perform. Constr. Fac.*, **10**(2), 47-56.

US DOT (U.S. Department of Transportation). (2007), *National Bridge Inventory*, http://www.fhwa.dot. gov/ bridge/mat07.xls, viewed on 25 October 2008.